Metallography, Microstructure, and Analysis (2020) 9:873–883
https://doi.org/10.1007/s13632-020-00702-w

TECHNICAL ARTICLE

Morphology and Nucleation of Intermetallic Phases in Casting Al–Mg–Si Alloys

Anna Slyudova[1] · Oleksandr Trudonoshyn[1,2] · Olena Prach[3] · Vitaliy Lisovskii[1]

Received: 11 September 2020 / Revised: 28 October 2020 / Accepted: 10 November 2020 / Published online: 3 December 2020

Abstract

The changes in the structure of Al–Mg–Si casting alloys after additional alloying are observed. In order to predict and to explain with greater confidence, the phase transformations in the studied alloys equilibrium phase diagrams were calculated using Thermo-Calc software. The results of the Thermo-Calc are in good agreement with the microstructure analysis. Morphology and chemical composition of intermetallic phases were investigated by scanning electron microscopy, energy-dispersive x-ray analysis, and electron probe microanalysis on polished and deep etched microsections. Several intermetallic phases with Fe and Mn, phases that contain Zn and Cu, and Al_3Ti crystals were described. It was found that the addition of Mn changes the morphology of Fe-containing intermetallics that improve strength and ductility of the alloys; crystals Al_3Ti can act as nucleating particles of α-Al dendrites; Cu and Zn lead to the formation of several fusible eutectic phases. To better understand the influence of the different intermetallics, the mechanical properties (Brinell hardness, ultimate tensile strength, yield strength, elongation) were measured. Alloying with Cu and Zn exhibits the best values of hardness and strength (up to 85 HB and UTC = 251 MPa), while the highest ductility was achieved in the alloy with composition Al–5.5Mg–2.5Si–0.6Mn (6.7%). Alloys possess the lowest properties (both strength and ductility) with the highest concentrations of Fe and Si (UTS up to 173 MPa with elongation 3.4%).

Keywords Aluminum alloys · Phase diagrams · Multistep nucleation · Microstructure · Intermetallics

Introduction

Despite widespread wrought Al–Mg–Si alloys (6000 alloys) in various industries, Al–Mg–Si casting alloys remain underestimated. However, Al–Mg–Si casting alloys have a number of advantages that make the alloys interesting for further development: high strength-to-weight ratio, a good combination of strength-ductility, good castability and formability, high corrosion resistance, age-hardening, high melting point of eutectic [1, 2].

In Al–Mg–Si alloys, Fe, Mn, Cu, Zn, and Ti can be present as impurities or can be used as alloying elements. Fe is the most common impurity in Al alloys, and, in most cases, Fe is considered an undesired impurity. Fe can form with Al and Si several types of intermetallics (α-AlFeSi, β-AlFeSi, etc.). β-phase has the most harmful effect on strength and ductility since it has acicular or platelet morphology with size up to several millimeters [3]. The possibility of improving mechanical properties by changing morphology of the Fe-containing intermetallics from needles to “Chinese script” or compact shapes was reported [4]. For most HPDC (high pressure die casting) alloys, Fe is limited by 0.2 wt.% to achieve high levels of ductility and toughness [5].

Mn is the most effective neutralizer for the negative impact of Fe on the mechanical properties of Al and its alloys. Fe is usually added to the HPDC Al alloys to prevent die-sticking. Mn (up to 0.6 wt.%) can be added to the alloys with high Mg content to replace the Fe for this purpose [6, 7]. Mn stimulates the formation of the compact (Fe, Mn)-containing phases and inhibits the formation of acicular-shaped Fe-containing intermetallics in the HPDC Al–Mg–Si

✉ Oleksandr Trudonoshyn
oleksandr.trudonoshyn@fau.de; oltrud@gmail.com

1 Department of Materials Science and Design Basics, Vyatskiy State University, Moscow Street 36, 610000 Kirov, Kirov Region, Russia

2 Materials Science Department, Friedrich-Alexander-Universität Erlangen-Nürnberg, Martensstraße 5, 91058 Erlangen, Germany

3 Technische Universität Darmstadt, Alarich-Weiss-Straße 2, 64287 Darmstadt, Germany

alloys. With the ratio Mn/Fe > 0.5, the predominant phase in the system is the compact α-phase [3]. It is also found that Mn addition in the amount of 0.6 wt% to Al–Mg–Si alloy can increase its properties (such as hardness, tensile, and yield strength) by 30% [8, 9].

Ti is a common impurity in Al alloys, and its compounds Al_3Ti, TiB_2 are often used [10, 11] as grain refiners for Al alloys. Cantor [12, 13] describes the adsorption model where Al-grains' heterogeneous nucleation occurs on adsorption layers of Al_3Ti formed on TiB_2 particles. Ti addition in small amounts does not show any significant impact on the mechanical properties of HPDC [14] as well as for PM (permanent mold) [15, 16] Al–Mg–Si alloys.

Zn addition to Al (combined with Mg and/or Cu) turns alloys to age-hardenable type with the highest strength [17, 18]. The effect of Zn on the Al–Mg–Si system is equivocal and not studied enough. Thus, Zn addition to the 6000 alloys does not show any noticeable effect [19, 20]. However, several recent researches [21–23] have shown significant enhancement in the strength characteristics (increase in UTS up to 30–40%) of the Al–Mg–Si casting alloys with Zn addition.

Cu is one of the most commonly used additions for Al–Mg–Si and has the most significant impact from all alloying elements on the strength characteristics of Al–Mg–Si alloys (but with a simultaneous decrease in ductility and corrosion resistance) [24, 25].

Even though the influence of the considered elements on alloys of the Al–Mg–Si system is well studied in the literature, these results are difficult to compare with each other (due to different casting methods or different composition of the base alloys). Therefore, in the current work, not only a more detailed study of the effect of these elements on the structure is carried out, but also the results of mechanical properties are presented to facilitate the comparison of their effects.

Materials and Methods

The chemical compositions of the studied alloys are represented in Table 1. As starting materials, high purity Al (A99.997), pure Zn (99%), and pre-alloys AlMg50, AlCu50, AlMn26, AlSi25, and AlTi10 were used. All starting materials were preheated before being transferred into an electric resistant furnace. The graphite crucibles were used for the melt preparation. The melt temperature was maintained at 720 ± 5 °C. The melt was degassed under Ar atmosphere for 10 min before casting.

Conventional metallographic techniques were used for sample preparation. The alloys' structure was evaluated by SEM (JSM-6510 LV, Japan) using secondary electrons (with SEI and LEI detectors). The phase composition was measured using SEM EDS (JSM-6510 LV with Energy-Dispersive Spectrometry systems). The EDX analysis was performed at an accelerating voltage of 15 kV on polished samples. A five-point analysis was conducted for each phase, and the average was presented as the measurement. The JEOL JXA-8100 (operating voltage—15 keV, a spot size—10 μm, a step size—0.25 μm, and a dwell time—500 ms) was used for the electron probe microanalysis (EPMA).

The thermodynamic and phase diagram calculations for multicomponent systems were performed by Thermo-Calc software using the TCAl2: Al alloys v2.1 database.

Results and Discussion

Influence of Fe and Mn

In order to understand the phase formation in the studied alloys, the multicomponent equilibrium phase diagrams in the sections Al–5.5Mg–2.5Si–xFe, Al–5.5Mg–2.5Si–0.6Mn–xFe, and Al–5.5Mg–xSi–0.6Mn are calculated and shown in Fig. 1.

The solubility of Fe in the solid α-Al in the current system is close to 0. Before Fe reaches the concentration of 2.0 wt% (Fig. 1a), the first crystallized phase is α-Al, and the crystallization range is stable. When the Fe content reaches

Table 1 Nominal chemical composition and mechanical properties of investigated alloys

	Chemical composition bal.-Al wt.%							Mechanical properties			
Alloy	Si	Fe	Cu	Mn	Mg	Ti	Zn	HB	UTS, MPa	YS, MPa	A, %
F	2.5	0.1	–	–	5.5	<0.1	–	70	189 ± 6	129 ± 4	3.6 ± 0.3
M	2.5	<0.1	–	0.6	5.5	<0.1	–	79	225 ± 4	159 ± 4	6.7 ± 1.1
S	4	<0.1	–	0.6	5.5	<0.1	–	71	173 ± 7	126 ± 3	3.4 ± 0.4
T	2.5	<0.1	–	0.6	5.5	0.2	–	74	221 ± 5	157 ± 5	5.2 ± 0.5
Z	2.5	<0.1	–	0.6	5.5	<0.1	1.8	83	245 ± 7	173 ± 5	4.6 ± 0.5
C	2.5	<0.1	1.5	0.6	5.5	<0.1	1.8	85	251 ± 6	176 ± 4	3.3 ± 0.4

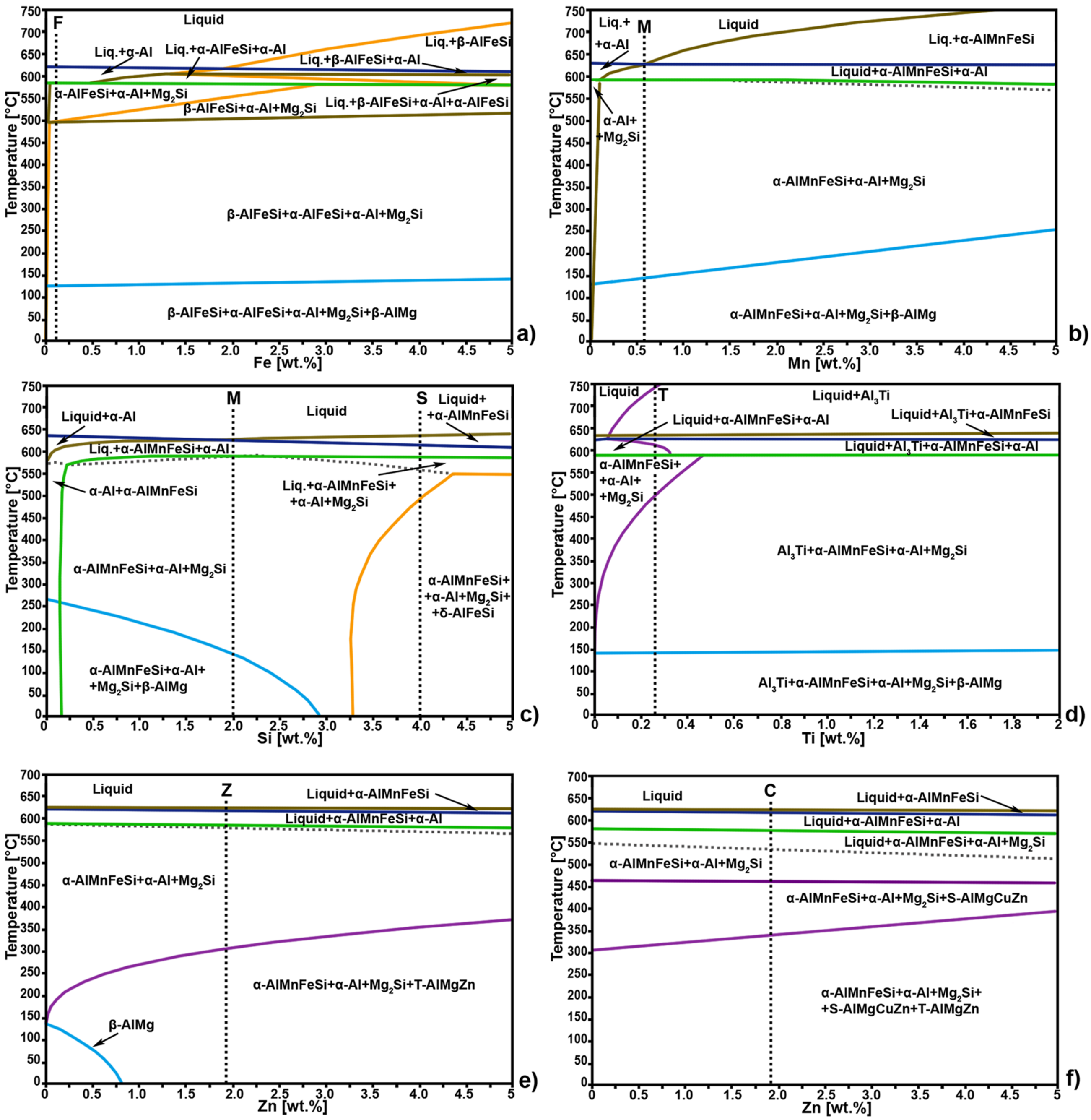

Fig. 1 Equilibrium diagrams **a** Al–5.5Mg–2.5Si–xFe; **b** Al–5.5Mg–2.5Si–0.6Mn–xFe; **c** Al–5.5Mg–2.5Si–*x*Mn–0.1Fe; **d** Al–5.5Mg–2.5Si–0.7Mn–*x*Ti; **e** Al–5.5Mg–2.5Si–0.6Mn–*x*Zn; **f** Al–5.5Mg–2.5Si–0.6Mn–1.5Cu–*x*Zn

above 2.0 wt%, the primary β-AlFeSi intermetallic phase was formed as a prior phase, followed by the α-Al phase formation. The solidification range of the Al–5.5 Mg–2.5Si–Fe alloy was increased from 38 °C (below 0.2 wt.% Fe) to 142 °C at 5 wt.% Fe.

The solubility of Mn in the solid α-Al in the current system varies from 0.12 wt.% at 590 °C (eutectic temperature) to 0.07 wt.% at 300 °C (Fig. 1b). Before the concentration of Mn reaches to the 0.6 wt.%, the first crystallized phase is α-Al, and the crystallization range is stable. When the Mn content is above 0.6 wt.%, the primary α-AlMnFeSi intermetallic phase was formed as a prior phase, followed by the formation of the α-Al phase. The solidification range of the Al–5.5 Mg–2.5Si–Mn alloy was increased from 41 °C (below 0.6 wt.% Mn) to 188 °C at 5.0 wt.% Mn.

Figure 1c shows the equilibrium phase diagram for the Al–5.5Mg–*x*Si–0.6Mn system. This section of the diagram can be divided into three areas: 1—with the excess of Mg, 2—near-equilibrium composition; 3—with the excess of Si. When the Si content was below 2.0 wt.%, the primary α-Al phase was formed as a prior phase, followed by the formation of the α-AlMnFeSi phase and then β-Mg_2Si. In excess of Mg area, the β-AlMg phase is formed. Alloys in this range have the next set of phases: α-Al + α-AlMnFeSi + β-Mg_2Si + β-AlMg. The second area lies between 2% and 3.3% of Si. The increasing of the Si content inhibits the formation of the β-AlMg phase. Alloys in this range have equilibrium pseudobinary hypoeutectic Al–Mg_2Si structure. The first crystallized phase in this area is the α-AlMnFeSi phase, followed by the formation of α-Al. The third area starts at 3.3 wt.% Si and is characterized by the increase in the solidification range. The first crystallized phase is still α-AlMnFeSi. The next two phases are α-Al and β-Mg_2Si. The last is Si-reach δ-AlMnFeSi phase. From the literature, it is known that this phase is brittle, acicular-shaped, and leads to a decrease in mechanical properties of Al–Mg–Si alloys in the as-cast state [8, 9].

The Thermo-Calc calculations results are well supported by the literature data [3, 26, 27] and by the microstructural analysis. The F alloy structure consists of α-Al dendrites, Al–Mg_2Si eutectic, and a few intermetallic compounds that can be identified as α-AlFeSi and β-AlFeSi (see Table 2). M alloy consists of α-Al dendrites, Al–Mg_2Si eutectic, and α-AlMnFeSi intermetallic phase.

Figure 3a–c shows the morphology of intermetallic α- AlFeSi and β-AlFeSi phases observed in F alloy. The α-AlFeSi has a compact eutectic structure, and the β-AlFeSi phase generally has a needle-shaped or plate-like form. Figure 3b also shows that the phases of β-AlFeSi, Mg_2Si, and α-AlFeSi can grow simultaneously, forming eutectic clusters. This means that the eutectic clusters were formed during the last stage of solidification (Fig. 2a) in the temperature range 585–586 °C.

The significant negative effect of the β-AlFeSi phase on the mechanical properties (see Table 1) is associated with its stress raising potential (due to its plate- and needle-shaped morphology) and its brittle nature [3]. Also, the intermetallic plates' presence increases shrinkage cavities during solidification and brittleness of alloys because of the blockage of the interdendritic channels, thus interfering with the flow of liquid metal to fill shrinkage cavities during solidification [28]. To neutralize this effect, Mn is used as an alloying element. Mn modifies the morphology of Fe-reach intermetallics in a rounded-shape, and irregular needle-shaped crystals turned into dendritic arms, irregular eutectic or compact hexagonal shape (Fig. 3) [29–31]. According to [26], α-AlMnFeSi phase is the most stable phase with a ratio Fe/Mn < 2.

A possibility of the nucleation of α-AlFeSi and β-AlFeSi on the oxidic particles and conglomerates is shown in the works [32, 33]. In the present research, no oxidic particle inside of these phases was found. Yang et al. [34] investigated the possibility of heterogeneous nucleation of α-Al on the primary α-AlMnFeSi intermetallics. It was concluded that α-AlMnFeSi particles are potential substrates for nucleation of α-Al dendrites in Al–5.3 Mg–2.4Si–0.6Mn–1.0Fe alloy [34]. In the studied Al–5.5 Mg–2.5Si–0.6Mn alloy (M alloy), two types of the α-AlMnFeSi phases were found (Fig. 3): single particles (or particles conglomerates) that tend to faceted (frequently hexagonal) morphology (Fig. 3d, e); eutectic (frequently with dendritic-arm morphology) phases (Fig. 3f–l).

First type (faceted particles) forms in case of crystallization of α-AlMnFeSi as a prior phase or simultaneously with α-Al in the temperature range 622–588 °C. Similar to the results [34], α-AlMnFeSi particles, in this case, can be potential substrates for nucleation of α-Al dendrites.

Table 2 EDX analysis of the intermetallics in the studied alloys

Phases	Alloys	Elements, at.%								
		Mg	Al	Si	Ti	V	Fe	Mn	Cu	Zn
α-AlFeSi	F	0.3	78.4	11.5	–	–	9.1	0.7	–	–
β-AlFeSi		0.2	69.7	16.2	–	–	13.3	0.5	–	–
α-AlMnFeSi	M	0.2	72.0	10.2	–	–	1.1	16.5	–	–
	S	0.3	73.0	12.2	–	–	1.3	13.1	–	–
	T	0.4	72.2	9.6	0.2	–	2.1	15.4	–	–
	Z	0.1	72.2	10.3	–	–	1.7	15.5	–	0.2
δ-AlMnFeSi	S	0.1	64.3	22.6	–	–	1.0	12.0	–	–
Al_3Ti	T	0.2	72.6	0.6	25.1	1.0	0.2	0.3	–	–
S-AlMgCuZn	C	13.6	60.4	0.6	–	–	–	–	24.3	1.0
α-AlMnFeCuSi		0.7	70.8	4.8	–	–	2.8	12.8	7.7	0.4
T-AlMgZn	C	28.6	48.6	0.1	–	–	–	–	0.2	22.4
	Z	30.2	46.2	0.2	–	–	–	–	–	23.4

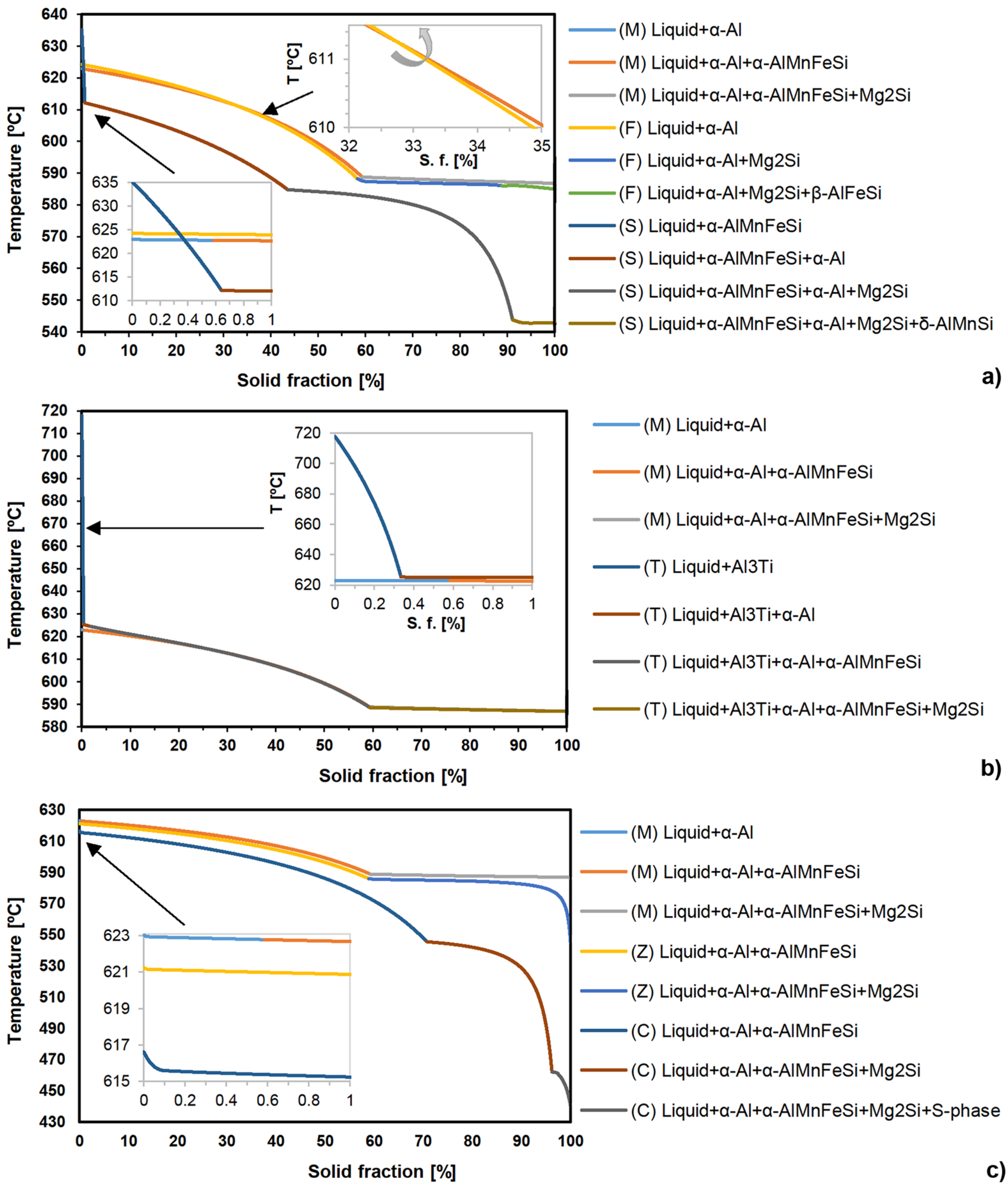

Fig. 2 Solidification curves of **a** F, M, S alloys; **b** M and T alloys; **c** M, Z, C alloys

The second type (eutectic phase) is more frequent in the structure due to Fe and Mn's low content in the M alloy leads to the crystallization of α-Al as a prior phase (Fig. 1b, d and e). During solidification, this may lead to pushing [35] Mn and Fe to the front of the solidification interface. Thus, the α-AlMnFeSi phases are mainly precipitate in the

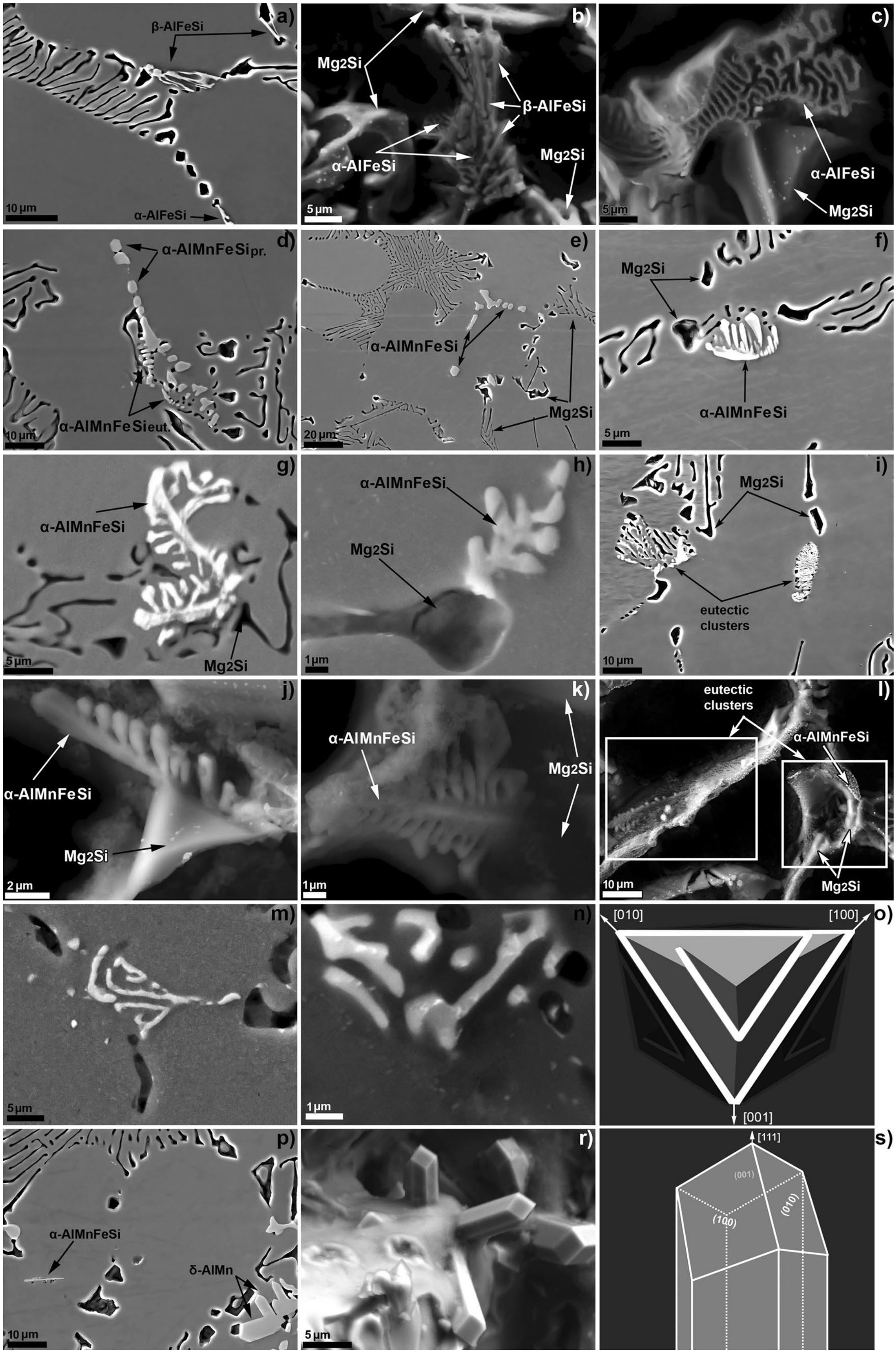

Fig. 3 Morphology of Al(Mn)FeSi phases: **a**–**c** intermetallics in F alloy; **d**–**n** intermetallics in M alloy; **p**, **r** intermetallics in S alloy; **o**, **s** volumetric models

interdendritic area and form eutectic clusters together with Mg_2Si (Fig. 3f, i and l).

The microstructural analysis (Fig. 3g, h, j and k) shows that the α-AlFeMnSi phase's nucleation can occur heterogeneously on lamellas and even on the primary Mg_2Si crystals. The phases are nucleated in such a way crystallized during the last stage (Fig. 2a) of the solidification, when all phases crystallize together in the temperature range 588–586 °C. Figure 2a shows that the addition of 0.6 wt.% Mn does not lead to significant changes in the solidification behavior.

Also, the α-AlMnFeSi phase with the morphology of triangular spirals (Fig. 3m and n) was detected. Such morphology may indicate that this α-AlMnFeSi phase has a volumetric octahedral morphology (Fig. 5o). It allows explaining the formation of such type morphology by the epitaxial growth, assuming that α-AlMnFeSi nucleated on the primary octahedral Mg_2Si crystal [7].

As reported in [8, 9], the increase in Si content in the Al–Mg–Si alloys leads to the formation of metastable polyhedral δ-AlMnSi phases. Figure 3p–s shows as-cast morphology and crystallographic indices of the δ-phase. Solution treatment promotes the dissolution of the metastable δ-AlMnFeSi phase and the formation of more stable phases (α-AlFeMnSi, β-AlFeSi) [8, 9]. As it was reported in [8, 9], the excess Si from the δ-phase dissolves in the α-matrix during the solution treatment process. The results of the volume fraction of the phases in the solid state are shown in Table 3.

Influence of Ti

In the previous work [15], the effect of Ti on the mechanical properties in the studied alloys was discussed. Figure d shows the phase diagram of the Al–5.5Mg–2.5Si–0.6Mn–*x*Ti. Ti has relatively middling solubility in Al and leads to the formation of Al_3Ti intermetallics [7, 15]. The peritectic concentration in the Al–5.5Mg–2.5Si–0.6Mn–Ti system is 0.47 wt.% Ti. During cooling, the solubility of Ti decreases rapidly and drops below value 0.1% at 400 °C and to near 0 at RT. α-Al crystallizes as the first phase before 0.06 wt.% Ti (area with a stable solidification range). When the Ti content increases above 0.06 wt.%, Al_3Ti intermetallic phase was formed as a prior phase (followed by the formation of α-AlMnFeSi and then α-Al phase and Mg_2Si phases) and so can act as substrates for the nucleation of, e.g., α-Al and Mg_2Si phases [7]. The liquidus temperature is increased with the further increase in the Ti concentration. The solidification range of the Al–5.5 Mg–2.5Si–0.6Mn alloy increases from 45 to 210 °C at 0.4 wt.% Ti.

The partition coefficient of Ti in the Al $K > 1$, and therefore the concentration of Ti increases from the boundary of Al grain to the center (unlike Mg and Si) [15]. It can be seen from Fig. 4b that the interdendritic area in the T alloy is poor with Ti. Figure 5 shows that Ti addition to the Al–5.5 Mg–2.5Si–0.6Mn alloy leads to the formation of Al_3Ti tetragonal particles (in the centers of equiaxial dendrites, see fig). Figure 5 represents the preferential morphology of the Al_3Ti crystals in T alloy. The morphology of the primary Al_3Ti crystals can be attributed to the hopper type. Figure 5d shows a volumetric model with crystallographic indices of Al_3Ti crystals in the as-cast state.

It has been reported [32, 33] that the oxide particles and oxide films are preferred sites for the nucleation of a large variety of phases. However, the α-Al dendrites could not nucleate directly on oxides due to the non-wettability [32, 33]. The wettability is one of the most critical points of the particle's possibility to act as a potential nucleus. Thus, it is necessary to use either catalyst that can promote the wetting force and the adsorption layers, or an intermediate intermetallic phase that wets the oxidic particles and, at the same time, can be wetted by Al to overcome the problem with wetting. In T alloy, the Al_3Ti phases can nucleate on the oxidic particles [7], but the possibility of nucleation of α-Al was not found.

Ti addition to the Al–5.5Mg–2.5Si–Mn alloy illustrates well the multistage heterogeneous nucleation. The Al_3Ti crystals can nucleate at the oxidic nucleating particles (Fig. 5d). The formed Al_3Ti crystals, in turn, can act as the nucleus for α-Al dendrites (Fig. 5a–c). However, if the concentration of Ti in the alloy exceeds the peritectic point, the Al_3Ti phase continues to grow, and Al_3Ti conglomerates can

Table 3 Volume fraction of the phases according to Thermo-Calc calculation, [%]

Phases	F	M	S	T	Z	C
α-Al	90.90	89.16	89.10	88.16	88.93	86.43
Mg_2Si	5.74	5.45	8.32	5.20	5.30	5.26
β-AlMg	3.10	3.66	–	4.12	–	–
β-AlFeSi	0.26	–	–	–	–	–
α-AlMnFeSi	–	1.71	1.69	1.94	1.68	1.72
δ-AlMnFeSi	–	–	1.88	–	–	–
Al_3Ti	–	–	–	0.56	–	–
T-AlMgZn	–	–	–	–	4.09	5.76
S-AlMgCu	–	–	–	–	–	0.83

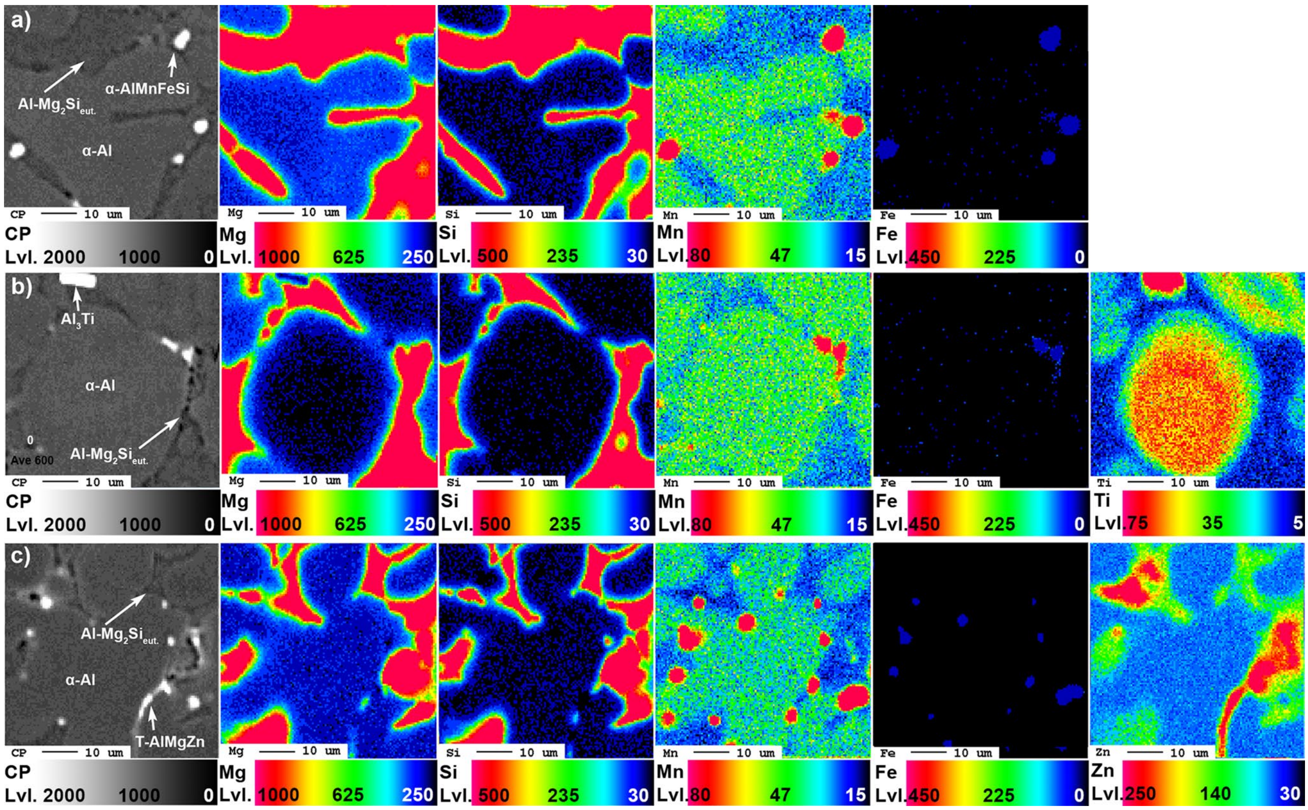

Fig. 4 EPMA maps **a** M alloy; **b** T alloy; **c** Z alloy

be formed (Fig. 5f). The density of the Al_3Ti compound is higher than the density of liquid Al. Therefore, Al_3Ti particles accumulate in the bottom of the crucible by gravitational settling [15, 36]. This effect entails that the formation of the Al_3Ti particles conglomerates, which, even during the intensive stirring, is not milled and stays in the metal after crystallization. The presence of conglomerates in the cast structure leads to the formation of additional stresses in the structure of the alloy, which negatively affects the mechanical properties, especially for thin-walled castings [15, 36].

Influence of Cu and Zn

Figure 1e and f shows changes in the equilibrium phase diagram on the cross section of Al–5.5Mg–2.5Si–0.6Mn and Al–5.5Mg–2.5Si–0.6Mn–1.5Cu with increase in Zn content. Unlike Ti, Mn, and Fe, Zn has very good solubility in the Al at evaluated temperatures. From the phase diagram Fig. 1g, it can be seen that Zn in the Al–5.5Mg–2.5Si–0.6Mn alloy is not involved in any high-temperature reactions but precipitates as T-AlMgZn phase in the solid state. The T-phase is stable in a huge homogeneity region with the stoichiometry $(Al,Zn)_{49}Mg_{32}$ [37–39]. The presence of Zn in the Al–Mg–Si alloy does not significantly affect the formation and morphology of the main phases (α-Al, Mg_2Si, α-AlMgFeSi) [18, 23]. However, it inhibits the formation of the β-AlMg phase. Addition of 1.5 wt.% Cu leads to the formation of one new phase (S-phase). Similar to the T-phase, S-phase forms in the solid-state precipitates from the α-Al matrix. Cu addition extremely increases the solidification range that negatively affects the porosity level of the castings. β-AlMg phase disappears with the addition of 1.5 wt.% Cu [37–39].

The T-AlMgZn phases are precipitated in solid state from the α-Al in-between Al–Mg_2Si eutectic cells and α-Al dendrites (Fig. 4c). Figure 6a–c shows the general microstructure of Z alloy and morphology of the eutectic Zn-containing T-phase. T-phase has the lowest formation temperature among the listed phases in this study. In work [23], it was showed that T-phase is sensitive to solidification and cooling rates.

Moreover, as can be seen from Fig. 6, the fragments of Mg_2Si eutectic and α-AlMnFeSi phase can act as a substrate for the nucleation of the T-phase. Thus, the mechanism of nucleation of Zn-containing can be attributed to the heterogeneous nucleation.

Figure 6d–f shows the general microstructure of C alloy and the phases that contain Zn and Cu. The presence of a small amount of Cu in the alloy with Zn [23] does not lead to the formation of new Cu-containing phases. In such a situation, the T-phase joined almost all Cu content. With higher

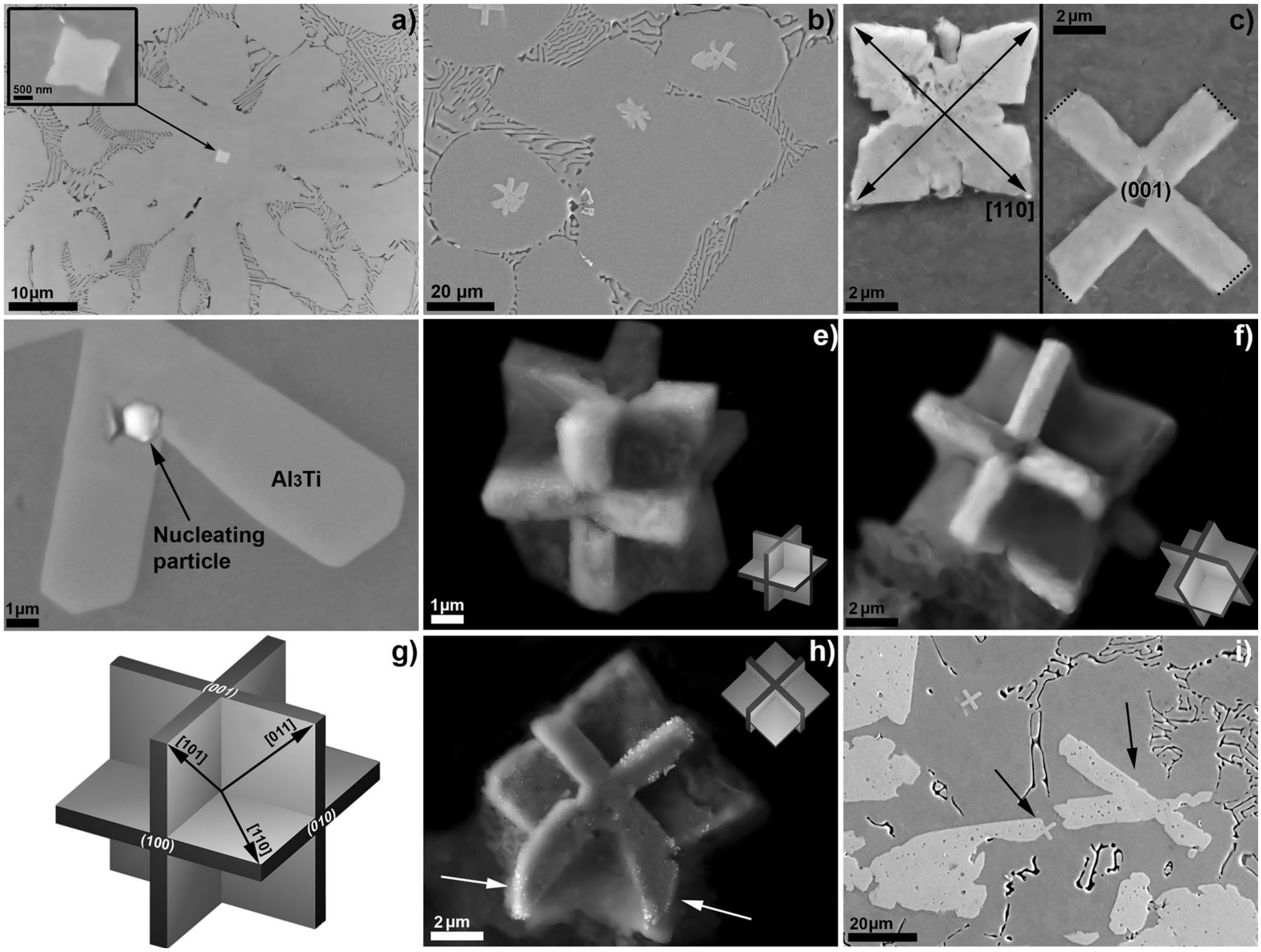

Fig. 5 Al3Ti crystals as a substrate for nucleation of α-Al dendrites (**a**–**c**), further growth of Al3Ti conglomerates (**d**–**e**) and nucleation of Al3Ti crystal on nucleation particle

Cu content, several new phases can be formed in the structure. Figure 8d shows that S-phase has eutectic morphology and grows close to the Mn-containing phase and forms a single structure. Since the Mn-containing phase formed earlier (Fig. 1h), it can be assumed that the α-AlMnFeSi phase becomes a substrate for heterogeneous nucleation S-phase on it. The results of EDX analysis are presented in Tab. 2.

Conclusions

Fe addition leads to the formation of the β-AlFeSi phase (needle-shaped and brittle), which leads to decreasing ductility of the alloy. Mn addition leads to the formation of α-AlMnFeSi intermetallics, which combines impurity Fe. This leads to the increasing ductility and other tensile properties of the alloy. The highest ductility was achieved in the alloy with composition Al–5.5Mg–2.5Si–0.6Mn (6.7%). The alloy without Mn shows one of the lowest levels of the properties (both strength and ductility) UTS up to 189 MPa with elongation of 3.6%.

Cu and Zn improve the hardness and strength of the alloys while impairing the ductility. S-AlCuZn and T-AlMgZn precipitate in the solid state from the α-Al matrix that promotes additional stress concentrators. Alloying with Cu and Zn exhibits the best values of hardness and strength (up to 85 HB and UTC = 251 MPa).

Acknowledgements Authors gratefully thank the center “ICDAM” and the Visegrad Fund for the support provided for the present research project. The authors are also thanking J.Hornik (ICDAM) and K.Mykhalenkov (NTUU “KPI”) for supervising the project.

Compliance with ethical standards

Conflict of interest No potential conflict of interest was reported by the authors.

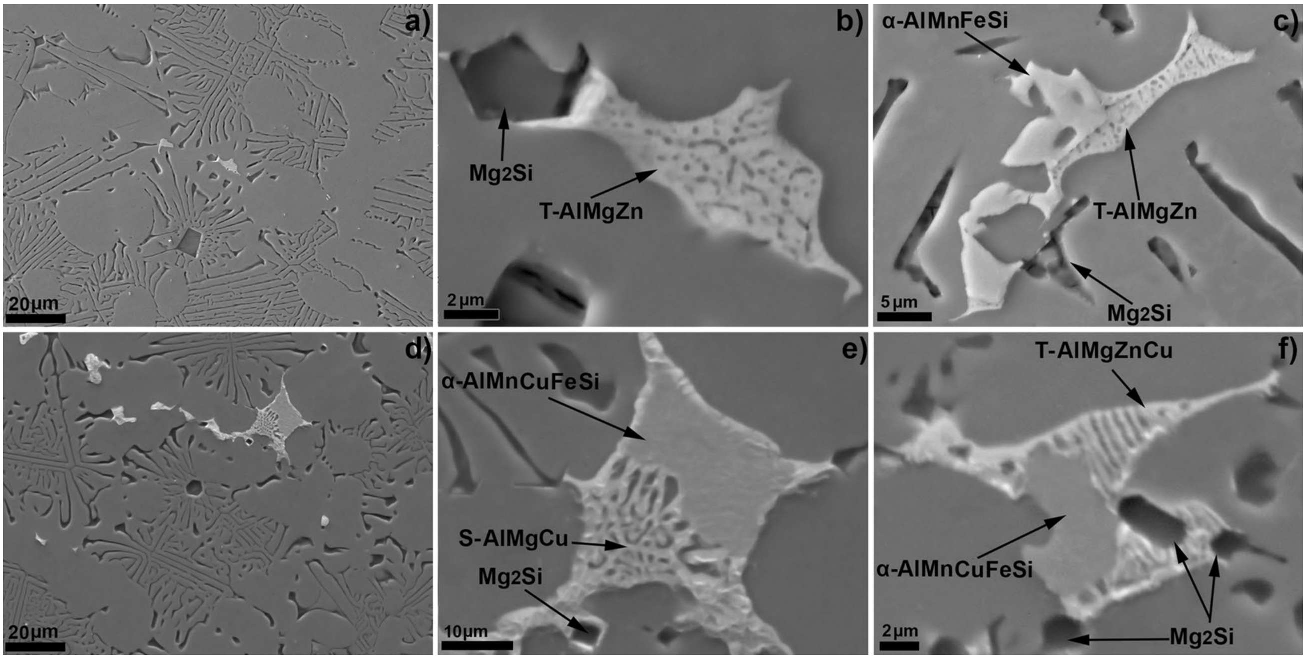

Fig. 6 Morphology of metastable Zn-containing and Cu-containing phases

References

1. O. Trudonoshyn, Studying the structure of Al-Mg-Si casting alloys doped by lithium. Phys. Met. Metall. **121**, 701–707 (2020). https://doi.org/10.1134/S0031918X2007011X
2. O. Prach, O. Trudonoshyn, P. Randelzhofer, C. Körner, K. Durst, Multi-alloying effect of Sc, Zr, Cr on the Al-Mg-Si-Mn high-pressure die casting alloys. Mater. Charact. (2020). https://doi.org/10.1016/j.matchar.2020.110537
3. S. Ji, W. Yang, F. Gao, D. Watson, Z. Fan, Effect of iron on the microstructure and mechanical property of Al-Mg-Si-Mn and Al-Mg-Si diecast alloys. Mater. Sci. Eng., A **564**, 130–139 (2013). https://doi.org/10.1016/j.msea.2012.11.095
4. K.Y. Wen, W. Hu, G. Gottstein, Intermetallic compounds in thixoformed aluminium alloy A356. Mater. Sci. Technol.. 19 (2003) 762–768. https://doi.org/10.1179/026708303225002839
5. J.E. Hatch, Aluminum Properties and Physical Metallurgy, ASM International, Ohio, 1984. https://doi.org/10.1361/appm1984p001
6. P. Zhang, Z. Li, B. Liu, W. Ding, L. Peng, Improved tensile properties of a new aluminum alloy for high pressure die casting. Mater. Sci. Eng., A **651**, 376–390 (2016). https://doi.org/10.1016/j.msea.2015.10.127
7. O. Trudonoshyn, O. Prach, A. Slyudova, V. Lisovskii, Structure formation and multistep nucleation in casting Al-Mg-Si alloys. Int. J. Cast Met. Res. **33**, 184–193 (2020). https://doi.org/10.1080/13640461.2020.1822632
8. O. Prach, O. Trudonoshyn, M. Puchnin, Effects of chemical composition on mechanical properties of Al-Mg-Si-Mn based alloys. Mater. Eng. Materiálové Inžinierstvo (MEMI). 24 (2017) 11–20. http://ojs.mateng.sk/index.php/Mateng/article/download/215/399
9. O. Trudonoshyn, M. Puchnin, O. Prach, Use of the ABI technique to measure the mechanical properties of aluminium alloys: Effect of heat-treatment conditions on the mechanical properties of alloys, Materiali in Tehnologije. 50 (2016). https://doi.org/10.17222/mit.2014.295
10. L. Arnberg, L. Backerud, H. Klang, Grain refinement of aluminium 2 : Intermetallic particles in master alloys for grain refinement of aluminium, Metals Technol.. (1982) 7–13. https://doi.org/10.1179/030716982803286368
11. B.A.L. Greer, P.S. Cooper, M.W. Meredith, W. Schneider, P. Schumacher, J.A. Spittle, A. Tronche, S. Park, Grain refinement of aluminium alloys by inoculation. Adv. Eng. Mater. (2003) 81–91. https://doi.org/10.1002/adem.200390013
12. B. Cantor, Embedded droplet measurements and an adsorption model of the heterogeneous nucleation of solidification. Mater. Sci. Eng., A **178**, 225–231 (1994). https://doi.org/10.1016/0921-5093(94)90547-9
13. B. Cantor, Heterogeneous nucleation and adsorption. Phil. Trans. R. Soc. Lond. A. **361**, 409–417 (2003). https://doi.org/10.1098/rsta.2002.1137
14. S.X. Ji, D. Watson, Y. Wang, M. White, Z.Y. Fan, Effect of Ti addition on mechanical properties of high pressure die cast Al-Mg-Si alloys. Mater. Sci. Forum **765**, 23–27 (2013). https://doi.org/10.4028/www.scientific.net/MSF.765.23
15. O. Trudonoshyn, M. Puchnin, K. Mykhalenkov, Features of structure formation and changes in the mechanical properties of cast Al-Mg-Si-Mn alloy with the addition of (Ti + Zr), Acta Polytechnica. 55 (2015) 282–290. https://doi.org/10.14311/AP.2015.55.0282
16. O. Trudonoshyn, O. Prach, V. Boyko, M. Puchnin, K. Mykhalenkov, Design of a new casting alloys containing Li or Ti + Zr and optimization of its heat treatment, in: *METAL 2014 - 23rd International Conference on Metallurgy and Materials, Conference Proceedings*, 2014: pp. 1399–1404. http://metal2014.tanger.cz/files/proceedings/17/reports/2750.pdf
17. R.S. Rana, R. Purohit, S. Das, Reviews on the influences of alloying elements on the microstructure and mechanical properties of aluminum alloys and aluminum alloy composites. Int. J. Sci. Res. Publ. 2 (2012) 1–7. https://pdfs.semanticscholar.org/c360/cdb98ac0c9d46e40640f877e931fb97257e1.pdf

18. Z. Li, Q. Wang, H. Tang, T. Liu, C. Lei, H. Jiang, W. Ding, Microstructure and mechanical properties of squeeze cast Al–5Mg–3Zn–1Cu–1Si alloy along cross section. Met. Mater. Int. (2020). https://doi.org/10.1007/s12540-020-00723-8
19. Y. Cai, C. Wang, J. Zhang, Microstructural characteristics and aging response of Zn-containing Al-Mg-Si-Cu alloy. Int. J. Miner. Metallurg. Mater. **20**, 659–664 (2013). https://doi.org/10.1007/s12613-013-0780-x
20. T. Saito, S. Wenner, E. Osmundsen, D. Calin, S.J. Andersen, J. Røyset, The effect of Zn on precipitation in Al-Mg-Si alloys. Phil. Mag. **94**, 2410–2425 (2014). https://doi.org/10.1080/14786435.2014.913819
21. L. Li, S. Ji, Q. Zhu, Y.U.N. Wang, X. Dong, W. Yang, S. Midson, Y. Kang, Effect of Zn concentration on the microstructure and mechanical properties of Al-Mg-Si-Zn alloys processed by gravity die casting. Metallurg. Mater. Trans. A. **49**, 3247–3256 (2018). https://doi.org/10.1007/s11661-018-4684-2
22. F. Yan, W. Yang, S. Ji, Z. Fan, Effect of solutionising and ageing on the microstructure and mechanical properties of a high strength die-cast Al-Mg-Zn-Si alloy. Mater. Chem. Phys. (2015) 1–9. https://doi.org/10.1016/j.matchemphys.2015.10.014
23. O. Trudonoshyn, S. Rehm, P. Randelzhofer, C. Körner, Improvement of the high-pressure die casting alloy Al–5.7Mg–2.6Si–0.7Mn with Zn addition. Mater. Charact. 158 (2019) 109959. https://doi.org/10.1016/j.matchar.2019.109959
24. I.J. Polmear, G. Pons, Y. Barbaux, H. Octor, C. Sanchez, A.J. Morton, W.E. Borbidge, S. Rogers, After Concorde: evaluation of creep resistant Al–Cu–Mg–Ag alloys. Mater. Sci. Technol. **15**, 861–868 (2013). https://doi.org/10.1179/026708399101506599
25. L.F.F. Mondolfo, *Aluminum alloys: structure and properties* (Butterworths, London, 1979)
26. S. Ji, D. Watson, Z. Fan, M. White, Development of a super ductile diecast Al-Mg-Si alloy. Mater. Sci. Eng., A **556**, 824–833 (2012). https://doi.org/10.1016/j.msea.2012.07.074
27. F. Yan, S.X. Ji, Z.Y. Fan, Effect of excess Mg on the microstructure and mechanical properties of Al-Mg2Si high pressure die casting alloys. Mater. Sci. Forum **765**, 64–68 (2013). https://doi.org/10.4028/www.scientific.net/MSF.765.64
28. M. Mahta, M. Emamy, X. Cao, J. Campbell, Overview of β-Al5FeSi phase in al-si alloys, in *Science Research Trends*, ed. by L.V. Olivante (Nova Science Publishers. Inc., New York, 2008), pp. 251–271
29. L. Liu,Y, B. Kang, S, The solidification process of Al–Mg–Si alloys, J. Mater. Sci.. 2 (1997) 1443–1447. https://doi.org/10.1023/A:1018545732009
30. C. Phongphisutthinan, H. Tezuka, T. Sato, Semi-solid microstructure control of wrought Al-Mg-Si based alloys with Fe and Mn additions in deformation-semi-solid-forming process. Mater. Trans. **52**, 834–841 (2011). https://doi.org/10.2320/matertrans.L-MZ201119
31. O. Prach, O. Trudonoshyn, P. Randelzhofer, C. Körner, K. Durst, Effect of Zr, Cr and Sc on the Al-Mg-Si-Mn high-pressure die casting alloys, Mater. Sci. Eng. A. 759 (2019) 603–612. https://doi.org/10.1016/j.msea.2019.05.038
32. Z. Fan, Y. Wang, Z.F. Zhang, M. Xia, H.T. Li, J. Xu, L. Granasy, G.M. Scamans, Shear enhanced heterogeneous nucleation in some Mg- and Al-alloys. Int. J. Cast Met. Res. **22**, 318–322 (2009). https://doi.org/10.1179/136404609X367452
33. J. Campbell, Entrainment defects. Mater. Sci. Technol. **22**, 127–145 (2006). https://doi.org/10.1179/174328406X74248
34. W. Yang, S. Ji, X. Zhou, I. Stone, G. Scamans, G.E. Thompson, Z. Fan, Heterogeneous nucleation of α-Al grain on primary α-AlFeMnSi intermetallic investigated using 3d sem ultramicrotomy and HRTEM. Metall. Mater. Trans. A **45**, 3971–3980 (2014). https://doi.org/10.1007/s11661-014-2346-6
35. S. Ji, F. Yan, Z. Fan, Development of a high strength Al-Mg2Si-Mg-Zn based alloy for high pressure die casting. Mater. Sci. Eng., A **626**, 165–174 (2015). https://doi.org/10.1016/j.msea.2014.12.019
36. C. Leyens, M. Peters, *Titanium and Titanium Alloys. Fundamentals and Applications*, 1st ed., Wiley-VCH GmbH & Co. KG a A, Koln, 2003
37. V. Raghavan, Al-Mg-Zn (Aluminum-Magnesium-Zinc). J. Phase Equilib. Diffusion **31**, 293–294 (2010). https://doi.org/10.1007/s11669-010-9684-x
38. V. Raghavan, Al-Mg-Si-Zn (aluminum-magnesium-silicon-zinc). J. Phase Equilibria Diffusion **32**, 72–74 (2011). https://doi.org/10.1007/s11669-010-9803-8
39. P. Liang, T. Tarfa, J. Robinson, S. Wagner, P. Ochin, M. Harmelin, H. Seifert, H. Lukas, F. Aldinger, Experimental investigation and thermodynamic calculation of the Al–Mg–Zn system. Thermochim. Acta **314**, 87–110 (2002). https://doi.org/10.1016/s0040-6031(97)00458-9